Society For Biomaterials

Reinforcing bioceramic scaffolds with *in situ* synthesized ε-polycaprolactone coatings

Francisco J. Martínez-Vázquez, Pedro Miranda, Fernando Guiberteau, Antonia Pajares

Departamento de Ingeniería Mecánica, Energética y de los Materiales, Universidad de Extremadura, Avda de Elvas s/n. 06006 Badajoz, Spain

Received 12 September 2012; accepted 14 February 2013
Published online 30 April 2013 in Wiley Online Library (wileyonlinelibrary.com). DOI: 10.1002/jbm.a.34657

Abstract: *In situ* ring-opening polymerization of ε-caprolactone (ε-CL) was performed to coat β-tricalcium phosphate (β-TCP) scaffolds fabricated by robocasting in order to enhance their mechanical performance while preserving the predesigned macropore architecture. Concentrated colloidal inks prepared from β-TCP commercial powders were used to fabricate porous structures consisting of a three-dimensional mesh of interpenetrating rods. Then, ε-CL was *in situ* polymerized within the ceramic structure using a lipase as catalyst and toluene as solvent, to obtain a highly homogeneous coating and full impregnation of in-rod microporosity. The strength and toughness of scaffolds coated by ε-polycaprolactone (ε-PCL) were significantly increased (twofold and fivefold increase, respectively) over those of the bare structures. Enhancement of both properties is associated to the healing of preexisting microdefects in the bioceramic rods. These enhancements are compared to results from previous work on fully impregnated structures. The implications of the results for the optimization of the mechanical and biological performance of scaffolds for bone tissue engineering applications are discussed. © 2013 Wiley Periodicals, Inc. J Biomed Mater Res Part A: 101A: 3551–3559, 2013.

Key Words: robocasting, scaffolds, PCL coating, *in situ* polymerization, mechanical properties

How to cite this article: Martínez-Vázquez FJ, Miranda P, Guiberteau F, Pajares A. 2013. Reinforcing bioceramic scaffolds with *in situ* synthesized ε-polycaprolactone coatings. J Biomed Mater Res Part A 2013:101A:3551–3559.

INTRODUCTION

Bone tissue engineering seeks to restore and maintain the function of human bone tissues using the combination of cell biology, materials science, and engineering principles.[1] The three main ingredients for tissue engineering are therefore, harvested cells, recombinant signaling molecules, and three-dimensional (3-D) matrices.[2] Cells and signaling molecules, such as growth factors, are incorporated to highly porous biodegradable scaffolds, which are subsequently implanted to repair bone defects by inducing and directing the growth of new bone.[3] Hence, the first and foremost function of a scaffold is its role as support structure that allows cells to attach, proliferate, differentiate, and organize into normal, healthy bone. In the engineering perspective, there are two general aspects to focus on a scaffold: the material (composition, grain size, etc.) and the pore architecture. These two aspects determine the mechanical (and also the biological) performance of the scaffold.[2]

An ideal scaffold has to meet stringent requirements in terms of biocompatibility, bioactivity, biodegradation, osteoinduction, pore architecture, mechanical performance, and so forth.[4] Unfortunately most materials are not simultaneously mechanically competent and bioresorbable, that is, mechanically strong materials are usually bioinert, while degradable materials tend to be mechanically weak,[5] especially when fabricated as porous structures.

Scaffolds require a significant level of pore interconnectivity to promote cell proliferation and diffusion of nutrients,[2,4,6] which in conventional fabrication techniques implies large volumetric porosities,[7] and thereby poor mechanical performance.[8,9] Direct writing techniques[10] such as robocasting (also known as microrobotic deposition) allow a much greater control on pore architecture, enabling the attainment of high interconnectivities at reduced total porosities. These techniques follow a layerwise fabrication scheme that allows one to build patient specific scaffolds by using medical scans data to generate the digital model for the fabrication process, so that the final implant can fit perfectly into the patient lesion. Robocasting is based on the robotic deposition of highly concentrated colloidal suspensions (inks) with minimal organic content capable of fully supporting their own weight during assembly.[11–13] Thus, a 3-D mesh of interpenetrating rods is built layer by layer by extrusion of the inks through the deposition nozzle following the pattern specified in the digital model.

Correspondence to: P. Miranda; e-mail: pmiranda@unex.es
Contract grant sponsor: Ministerio de Ciencia e Innovación (Programa FPU)
Contract grant sponsor: Junta de Extremadura and FEDER funds; contract grant number: IB10006

© 2013 WILEY PERIODICALS, INC.

Tricalcium phosphate (TCP, $Ca_3(PO_4)_2$) bioceramics exhibit a high biodegradability (resorption rate) and osteoconductivity, which makes them optimal scaffold materials from a biological point of view. However, despite improvements provided by robocasting, TCP scaffolds still exhibit insufficient mechanical resistance to be suitable for load-bearing applications.[14] One alternative to overcome this hurdle is adding a biodegradable polymeric phase to the scaffolds in order to develop a composite material with enhanced toughness[15,16] and strength.[16,17] It is worth to mention that an additional advantage of incorporating a polymeric material is the possibility to use it as a vehicle for biomolecules (growth factors, antibiotics, anti-inflammatory drugs, etc.), for controlled delivery.

On previous works, full impregnation of robocast scaffolds with biodegradable polymers has been demonstrated to be an excellent means to improve their mechanical performance.[18,19] The strengthening achieved in fully impregnated structures was attributed to two mechanisms: stress shielding and defect healing. The former is produced by the polymer occupying the predesigned macropores, which sustains part of the load thus reducing the stresses on the ceramic rods, whereas the latter is due to the impregnation of the rods micropores, which makes it harder to initiate a crack from these defects. Besides, the presence of a continuous ductile polymeric phase produces also a significant toughening of the structure[19] by means of a crack bridging mechanism.[15,16] Nonetheless, the interconnectivity of the pore structure is lost when the polymer fills the macropores. Thus, the aim of this work is to produce a biodegradable polymer coating on the ceramic rods to reinforce the scaffold without jeopardizing its pore interconnectivity.

The coating method proposed in this work consists of the *in situ* polymerization (ISP)[20–24] of ε-caprolactone (ε-CL), using an enzymatic catalyst[25,26] and an appropriate solvent concentration, since solventless conditions yield fully impregnated structures.[19] Thus, once the coating process was optimized, polycaprolactone (PCL)-coated TCP robocast scaffolds were fabricated by ISP and their microstructures and mechanical properties were analyzed and compared to those of bare scaffolds and fully impregnated structures prepared by ISP.[19]

EXPERIMENTAL PROCEDURE

Robocast scaffolds preparation

A commercially available Ca-deficient β-TCP powder (Fluka, Buchs, Switzerland), pre-calcined at 1300°C to obtain a final 84 wt % β-TCP/16 wt % calcium pyrophosphate composition[27] and attritor milled to around 1 μm particle size, was used to prepare inks for robocasting with a final solid content of 45 vol %, following a procedure similar to that of previous works.[12,14] First, a stable suspension was prepared by dissolving 1.5 wt % (relative to powder content) Darvan® C dispersant (R.T. Vanderbilt, Norwalk, CT) in distilled water, and the β-TCP powder gradually added. An appropriate amount (7 mg/mL of liquid in the final suspension) of predissolved hydroxypropyl methylcellulose (Methocel F4M; Dow Chemical Company, Midland, MI) was then added to the mixture to increase viscosity. Subsequently, the ink was gellified by adding 2 vol % (relative to liquid content) of polyethylenimine as flocculant. After each addition, the mixture was placed in a planetary centrifugal mixer (ARE-250; Thinky Corp., Tokyo, Japan) for a few minutes to improve its homogeneity and stability.

3-D β-TCP scaffolds consisting of a mesh of ceramic rods were constructed layer by layer via direct-write assembly of the ink using a robotic deposition device (3-D Inks, Stillwater, OK). The printing syringe was partially filled with the ink and placed on the 3-axis motion stage, controlled independently by a computer-aided direct-write program (Robocad 3.0; 3-D Inks). The ink was deposited through conical polymeric deposition nozzles (EFD, East Providence, RI) with a tip diameter $d = 250$ μm, at a printing speed of 30 mm/s. Each layer in the computer 3-D model of the structure consisted of parallel rods with a spacing from center to center $s = 500$ μm. Rods in adjacent layers were perpendicularly oriented and the layer height was set to $h = 175$ μm. The external dimensions of the scaffolds were set at about 17 mm × 17 mm × 10 mm so that a total of 60 layers were deposited. The deposition was done in a paraffin oil bath to prevent nonuniform drying during assembly.

The samples were removed from the bath and dried in air at room temperature for at least 24 h, and then heated at 400°C (1°C/min heating rate) for 1 h to evaporate organics. They were finally sintered at 1200°C (heating rate 3°C/min) for 2 h. These are optimal processing conditions for this particular type of powders.[27]

In situ polymerization

Enzymatic ring-opening polymerization[28] of ε-CL (monomer) was carried out within selected scaffolds to develop a polymeric film on the ceramic rods. Commercial ε-CL and anhydrous toluene were obtained from Aldrich Chemical Co. and were first dried over calcium hydride and then distilled under reduced pressure. Novozym 435—*Candida antarctica* lipase B immobilized on cross-linked polymethylmethacrylate beads—was purchased from Novozymes A/S and dried following a procedure described elsewhere.[29]

Novozym 435 (120 mg) and the selected TCP scaffold were dried in the reaction flask over molecular sieves at 40°C overnight in a vacuum oven. After drying, the oven was opened under nitrogen flow. A flask containing Novozym 435 and the ceramic sample was stoppered with a rubber septum and placed in an oil bath at 60°C—this temperature has been shown to produce polymers with maximal monomer conversion and molecular weight.[30] Then, the monomer (6 mL) and toluene (12 mL) were added by syringe through the septum under nitrogen atmosphere. The initial water content in all reactions was kept below 0.003 wt %.

After stirring the mixture for 72 h at the prescribed temperature, the reaction was stopped by retrieving the sample from the flask. The coated ceramic structure was immediately placed for 48 h in a vacuum oven at 60°C and 0.1 bar to evaporate the solvent.

Microstructural characterization

As-cut bare TCP scaffolds were observed by scanning electron microscopy (SEM, S-3600N; Hitachi, Tokyo, Japan), to analyze the original microstructure. The different dimensions of the bare structures (d, s, and h) were directly measured on appropriate section micrographs. The morphology of PCL-coated structures was analyzed also by SEM observations on transversal fracture surfaces, obtained by bending, to avoid polymer relocation during cutting. For a better subsurface analysis of coated struts a dual beam focused ion beam (FIB)/SEM microscope (Quanta 3-D FEG; FEI Co., Eindhoven, the Netherlands) was used to image polished transversal sections of selected rods.

Total porosity of these samples was evaluated by simple weighting and external dimensions measurements, and the closed porosity was determined from the apparent density measured by He-pycnometry considering a theoretical density for β-TCP of 3.07 g/cm^3.[27] The predesigned macroporosity was approximately estimated from geometrical considerations assuming perfectly interpenetrating cylinders and using the dimensional parameters evaluated by SEM.

Mechanical characterization

Rectangular parallelepiped specimens with dimensions of around 3 mm × 3 mm × 6 mm were cut from the PCL-coated structures for mechanical characterization by uniaxial compression tests. These tests were carried out on a universal testing machine (AG-IS10kN; Shimadzu Corp., Kyoto, Japan), in air, at a constant crosshead speed of 0.6 mm/min. Tests were performed in the direction perpendicular to the printing plane (i.e., orthogonal to the rod axes), which has been shown to be a weak direction in these ceramic structures.[14,31] Engineering stress–strain curves were calculated through normalization of captured load versus displacement data using the initial external dimensions of each sample. The compressive strength of the structure was estimated as the maximum stress applied in each test. A total of around 20 samples were tested in order to get statistically reliable values. Weibull statistics[32] were used to analyze the resulting strength data. Toughness was estimated as the strain energy density at two strain values: strain at compressive strength (G_{max}) and 10% strain ($G_{0.1}$), from the corresponding integrals of the nominal stress–strain curves. The data obtained were thoroughly compared to results for the bare and fully impregnated structures, obtained under the same experimental conditions, from a previous work.[19]

Intrinsic mechanical properties of the coated rods were also evaluated. Instrumented indentation (Nanotest, Micro Materials, Wrexham, UK) was used to determine their elastic modulus and hardness. The indentation tests were performed using a diamond Berkovich indenter on polished transversal sections (to 1 μm finish) of the coated scaffolds. Single indentations of about 5 μm depth were placed at the center of scaffold rods sections. The indent size (~35 μm) was small enough to avoid the influence of adjacent free surfaces.

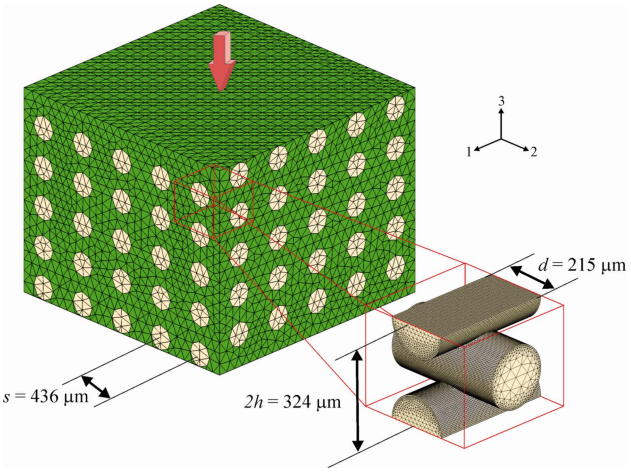

FIGURE 1. Finite element model used to simulate the uniaxial compression of bare, coated and fully impregnated scaffolds. The dimensions of the elements are around 100 μm, except in the interior unit cell shown in the insert where the dimension is reduced to ~ 3 μm at the rod surfaces. [Color figure can be viewed in the online issue, which is available at wileyonlinelibrary.com.]

Numerical modeling (FEM)

Finite element simulations were carried out using ABAQUS/Standard® software (Dassault Systèmes Simulia Corp., Providence, RI) to calculate the stress field developed under compression tests in bare, coated and fully impregnated scaffolds, in order to quantify the effect of stress reduction on the ceramic skeleton provided by the PCL polymer on the macropores, as would be explained in subsequent sections. The algorithm models the compression of a rectangular parallelepiped scaffold/infiltrate composite with approximate external dimensions 2 mm × 2 mm × 1.6 mm, as shown in Figure 1. The scaffold model consisted of 10 alternating orthogonal layers of parallel β-TCP rods with the following dimensions: rod diameter, d = 215 μm, in-layer rod spacing, s = 436 μm, and layer height, h = 162 μm, which are the average final dimensions of the sintered structures. The FEM grid for the scaffold system consisted of nearly six million quadratic tetrahedral elements. The dimensions of the elements are not uniform throughout the model. Element size is around 100 μm for most of the model, but much smaller within the central unit cell depicted in Figure 1, in which elements in the vicinity of the external surfaces of the ceramic rods have a minimum dimension of ~3 μm.

Isotropic elastic behavior is assumed for the entire system since, as it will be shown, fracture of the ceramic skeleton occurs before significant deviation from linearity is observed in the stress–strain curves of the composite scaffolds. The elastic properties from Table I were used as input parameters for the simulation of each individual material (i.e., TCP and TCP/PCL rods, and PCL infiltrate). For the simulation of bare and coated scaffolds, the corresponding rod values were used and a negligible elastic modulus was set for the infiltrating material (dark regions in Fig. 1). Since interfacial fracture has not been observed as a primary damage mode in polymer infiltrated robocast structures,[18,19]

TABLE I. Mechanical Properties of the Individual Materials, With Standard Deviations as Error

	E (GPa)[a]	H (GPa)[a]	ν
TCP/PCL rod	19 ± 2	0.8 ± 0.2	0.28[b]
TCP rod	16 ± 2[c]	0.7 ± 0.1[c]	0.28[b]
PCL	1.5 ± 0.2[c]	0.07 ± 0.02[c]	0.47[d]

[a] Obtained from instrumented indentation tests.
[b] Assumed equal to that of bulk TCP, from the literature.[33]
[c] From previous work.[19]
[d] From the literature.[34]

the bonding strength at the scaffold–infiltrate interface was considered infinite.

Boundary conditions were set as follows: the bottom surface of the structure is fixed while the top one is free to move in the normal direction with a defined displacement of 8 μm. The applied load was calculated as the sum of the reaction force at every node on the top surface of the structure and was then normalized by the initial surface area to get the nominal applied stress.

RESULTS

Shown in Figure 2 are representative scanning electron micrographs of the bare β-TCP robocast scaffolds after sintering. Both the macroscopic predesigned porosity [Fig. 2(a)] and the internal rod microporosity [Fig. 2(b,c)] are apparent. The mean dimensions of the ceramic structure as determined from the SEM observations were rod diameter, $d = 215 \pm 8$ μm, in-layer rod spacing, $s = 436 \pm 10$ μm, and layer height, $h = 162 \pm 5$ μm. According to the density measurements the total porosity in the β-TCP scaffolds is 66 ± 3%, with 4.0 ± 0.3% being closed porosity. Predesigned macroporosity was calculated to be ∼50%, so that rod microporosity would represent ∼16% of the sample volume, with ∼12% being accessible for polymer infiltration.

Figure 3 shows scanning electron micrographs of representative specimens of β-TCP robocast scaffolds before [Fig. 3(a)] and after coating by ISP of PCL [Fig. 3(b)]. A similar image for the scaffolds after full impregnation with PCL by ISP from a previous work[19] is included in Figure 3(c). These micrographs confirm that ISP is suitable to fabricate hybrid ceramic/polymer robocast structures, where the polymer either fully infiltrates the structures [Fig. 3(c)] or simply coats the ceramic bars [Fig. 3(b)]. Fully impregnated structures can be obtained under solventless infiltration conditions,[19] while the deposition of a homogeneous ε-PCL coating on the ceramic rods surface requires an appropriate solvent concentration (1:2, monomer:toluene ratio). Under this condition, a uniform film is created and the macroporosity of the structure remains unaltered, with the exception of some rounding of the pore channels produced by accumulation of the polymer at the intersections between TCP rods [Fig. 3(b)]. The coating morphology can be seen more clearly in Figure 4: the polymer properly coats the rods, creating a smooth surface [compare Figs. 4(a) and 2(b)], with a film of ∼0.2 μm minimum thickness [Fig. 4(b)]. Moreover, PCL also penetrates into the rods' microporosity, as it is clearly evident in the FIB section micrograph of Figure 4(c) [cf. Fig. 2(c)]. Indeed, for the PCL-coated structures, the porosity of the sample is reduced to 52 ± 3 vol %, indicating that a 14 ± 3% of the sample volume has been occupied by polymer, which is in excess of the estimated available rod open microporosity (∼12%). Excess polymer would produce the exterior polymeric film's and the observed accumulation of polymer at the rods intersections [Fig. 3(b)]. The extraordinary level of infiltration that can be achieved by ISP was already evidenced in

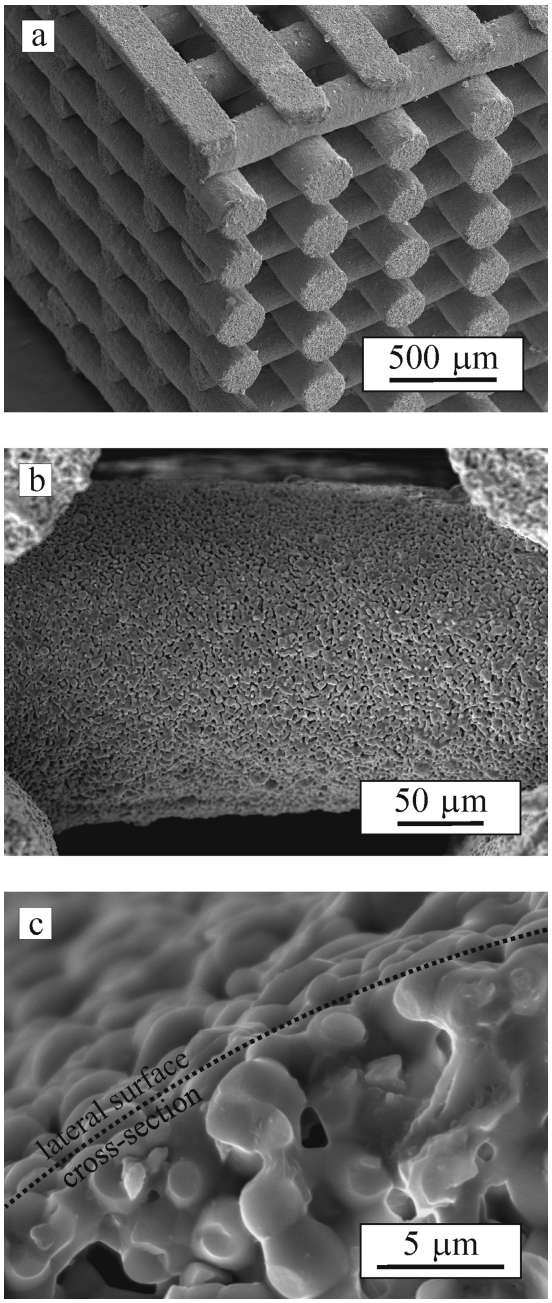

FIGURE 2. Scanning electron micrographs of the β-TCP robocast scaffolds before impregnation: representative as-cut specimens (a), rod surface, and transversal section details (b and c). Both the macroscopic, predesigned porosity, and internal rod porosity are evident.

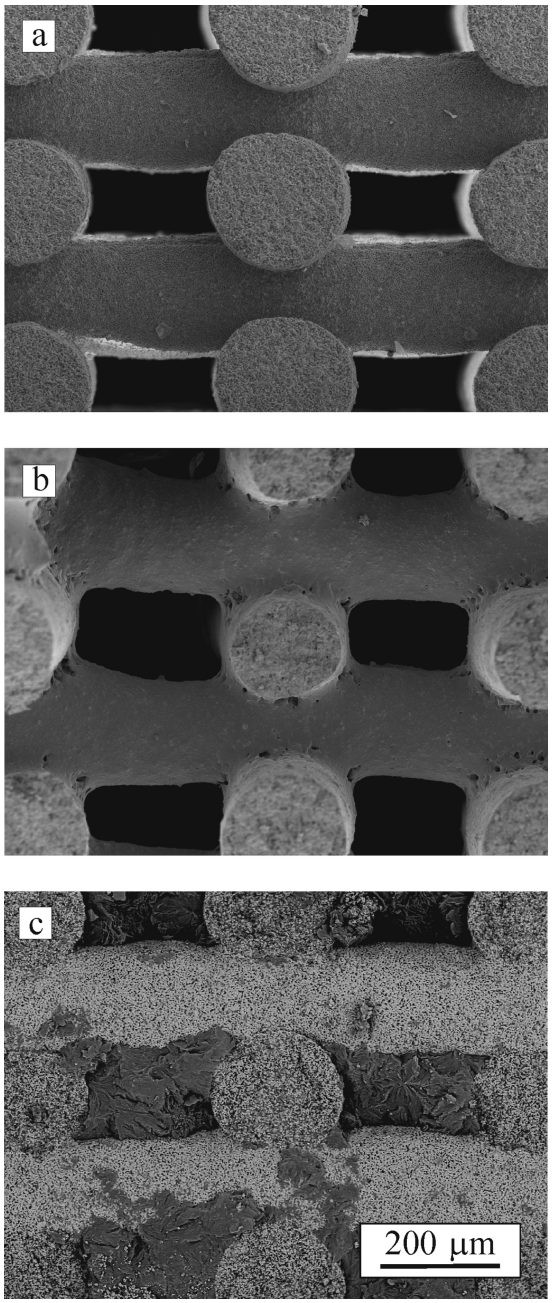

FIGURE 3. Scanning electron micrographs showing the microstructure of representative fracture surfaces of (a) bare β-TCP robocast scaffolds, (b) PCL-coated scaffolds, and (c) PCL fully impregnated structures (from previous work[19]). Backscattered electrons were used in (c) to obtain a better contrast between the polymeric and ceramic phases.

previous work,[19] where it was demonstrated that all the scaffold open porosity (62 ± 3%) was occupied by polymer in the fully impregnated structures [cf. Fig. 3(c)].

The mechanical properties of the different microstructural components of the structures shown in Figure 3, individual rods (bare TCP and TCP/PCL rods) and inter-rod polymer (PCL), are included in Table I. Data for the bare rods and the infiltrating polymer are from a previous work.[19] Poisson ratios for the different individual materials were obtained from the literature, as indicated. The elastic properties in Table I were used in the FEM simulations. Infiltration with polymer produced a slight increase (~20%, statistically significant, $p < 0.05$) in the rod modulus due to the PCL occupying the in-rod microporosity.

Regarding the mechanical properties of the scaffolds, Figure 5 shows a nominal representative stress–strain curve for uniaxial compressive tests performed on PCL-coated (TCP/PCL^C) hybrid structures. The data is compared to results for the bare β-TCP scaffolds (TCP), as well as PCL

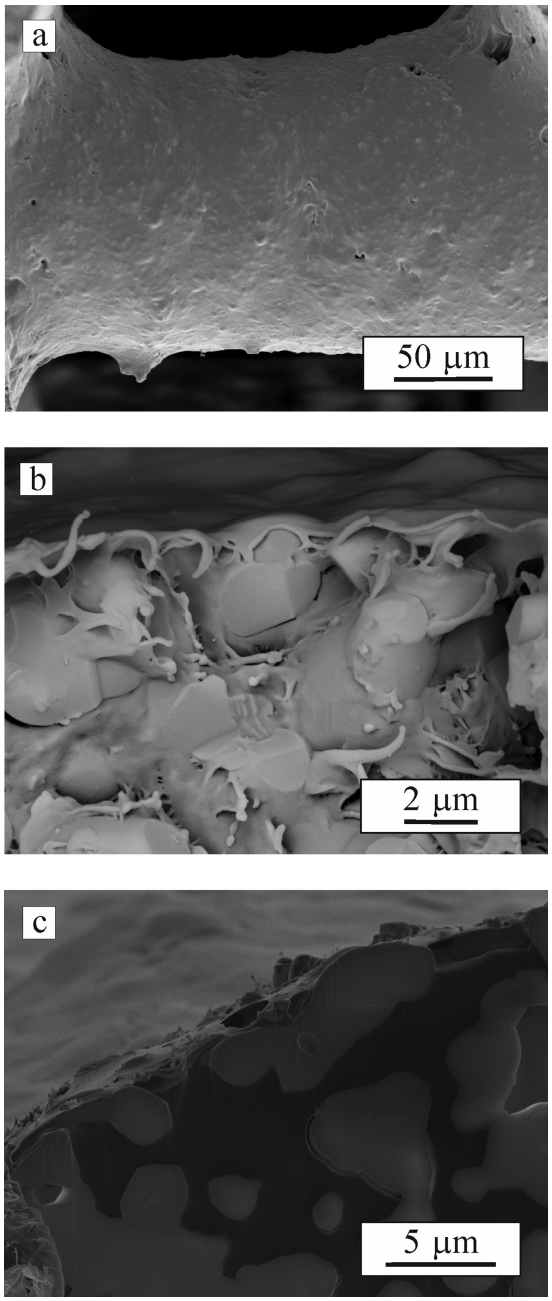

FIGURE 4. Scanning electron micrographs of a representative PCL-coated scaffold: (a) coated rod surface, (b) backscattered electron image of a fractured rod surface, and (c) FIB rod section micrograph. Dark regions in (c) correspond to PCL.

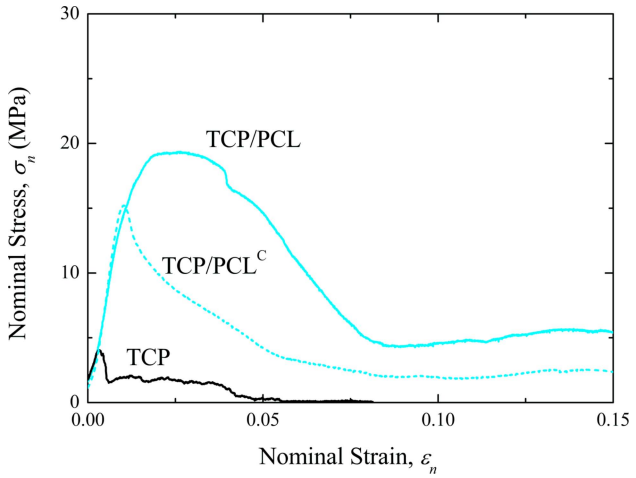

FIGURE 5. Representative nominal stress–strain curves obtained during uniaxial compression tests performed along the direction orthogonal to the rod layers on robocast β-TCP scaffolds coated with PCL (TCP/PCL^C). Data for bare scaffold (TCP) and fully impregnated structures (TCP/PCL) from previous work[19] are included for comparison. [Color figure can be viewed in the online issue, which is available at wileyonlinelibrary.com.]

fully impregnated hybrid structures (TCP/PCL) from previous work.[19] For each type of material, there is some variability in the shape of the curve from sample to sample, but the examples shown are representative in terms of area and maximum values. A noticeable increase on the strain energy density is evident upon either full infiltration or coating with PCL. Besides, a considerable improvement in the compressive strength of the TCP scaffolds is also apparent in both hybrid structures.

The strengthening effect of polymer infiltration is more clearly evidenced in the Weibull plots of Figure 6. This plot shows the failure probability as a function of applied compressive stress for TCP, TCP/PCL, and TCP/PCL^C scaffolds

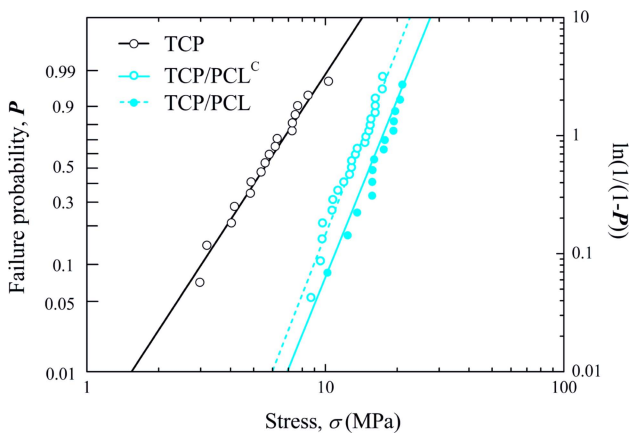

FIGURE 6. Weibull compressive strength plot (i.e., failure probability vs. applied stress) for PCL-coated structures (TCP/PCL^C). Data for bare (TCP) and PCL fully impregnated (TCP/PCL) structures from previous work[19] are included for comparison. The straight lines are linear fits to data using a Weibull probability function. [Color figure can be viewed in the online issue, which is available at wileyonlinelibrary.com.]

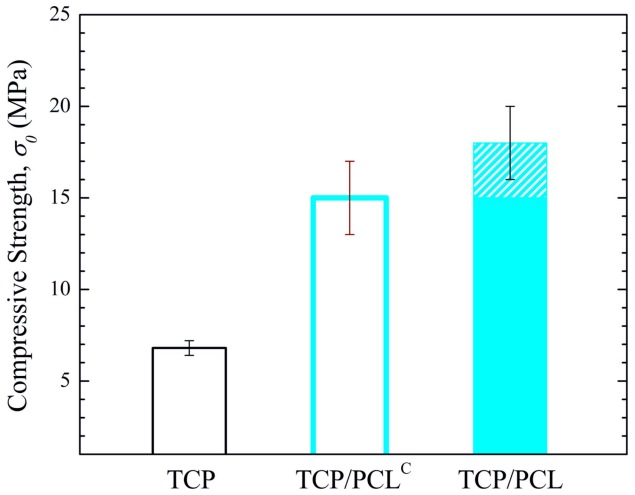

FIGURE 7. Compressive strength (central value, σ_0, of Weibull distribution) of PCL-coated (TCP/PCL^C) structures. Data for bare (TCP) and PCL fully impregnated (TCP/PCL) structures from previous work[19] are included for comparison. Error bars represent standard errors in the estimation of σ_0 and are not related to strength data scattering. The strength attributed to stress shielding in TCP/PCL structures is included as a white pattern in the corresponding bar (see "Discussion" section). [Color figure can be viewed in the online issue, which is available at wileyonlinelibrary.com.]

(again, data for TCP and TCP/PCL structures is taken from previous work[19]). Data correspond to individual compression tests and the straight lines are the best fits to data using the Weibull probability function[32]:

$$P = 1 - \exp[-(\sigma/\sigma_0)^m] \quad (1)$$

with P being the failure probability, and where the Weibull modulus, m, and central value, σ_0, are adjustable parameters.

Figure 7, compares the compressive strength (σ_0) measured in TCP/PCL^C scaffolds to the corresponding values for TCP and TCP/PCL structures from previous work.[19] It is clear that the compressive strength of the scaffolds is more than doubled in the case of PCL coating and nearly tripled upon full impregnation with PCL.

On the other hand, in terms of reliability, according to Figure 6, the hybrid structures exhibit an enhancement over the bare scaffolds which is similar for both types of hybrid structures, as evidenced by their similar Weibull modulus ($m = 5.2 \pm 0.2$ for TCP/PCL^C and $m = 5.0 \pm 0.3$ for TCP/PCL composites, versus $m = 3.1 \pm 0.1$ for TCP bare scaffolds).

The analysis of these strength data can be made in the light of the stress field generated in the scaffolds under uniaxial compression, as calculated by FEM. Figure 8 shows the evolution of the maximum tensile stress in the system as a function of nominal applied stress (i.e., applied load normalized by external section in the FEM model) for bare TCP, TCP/PCL^C, and TCP/PCL structures. The data for bare TCP and TCP/PCL^C are coincident since variation of the rod modulus does not affect the intensity of the stresses at a given load (although the strains, obviously, change). The

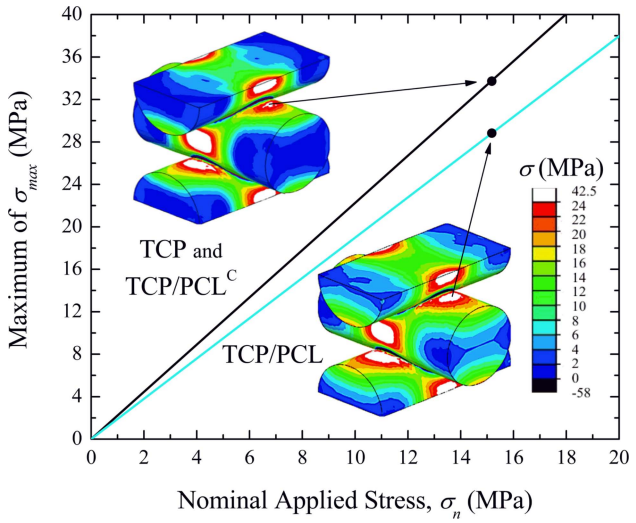

FIGURE 8. Plot of maximum tensile stress in the scaffold versus the nominal applied stress (applied load normalized by initial cross-sectional area) for bare TCP, coated TCP/PCL^C (coincident data, dark line), and TCP/PCL (light line). The FEM stress contours of the maximum tensile stress at each point of the structure at 15 MPa (black dots) of nominal applied stress are included to clarify the location of the maxima whose values are represented in the curves. [Color figure can be viewed in the online issue, which is available at wileyonlinelibrary.com.]

FEM-calculated stress contours (at indicated applied stress) corresponding to the maximum tensile stress, σ_{max}, at each point on the rod surfaces for each system are shown as an inset. These contours indicate the location of the maxima, close to the joints between rods, which are responsible for crack initiation.[35] It can be clearly seen that PCL full impregnation reduces the intensity of the maximum stress in the ceramic rods only slightly (by 17 ± 3%).

For the quantification of the toughening effect of PCL infiltration, Figure 9, shows the strain energy density at two strain values: strain at compressive strength (G_{max}) and 10% strain ($G_{0.1}$) for all three materials. Independently of the strain considered, PCL-coating of the scaffolds produces at least a fivefold increase in the toughness, while full impregnation of the structures is even more effective.

DISCUSSION

According to the scanning electron micrograph of Figures 3(b) and 4, it is possible to state that ISP of ε-PCL is a suitable polymer coating method for robocast scaffolds, providing a good approach to maintain the designed macroporosity, but fully impregnating the rod microporosity, thus producing a considerable enhancement of the mechanical behavior over bare scaffolds, as evidenced in Figures 6, 7, and 9.

As already mentioned in the "Introduction" section, the enhancement reported in fully impregnated, TCP/PCL, structures (a factor of strengthening of 2.6 ± 0.4) can be attributed to two concurrent mechanisms: (i) stress shielding by the polymer in the macropores which sustains part of the load, thus reducing the stresses in the ceramics rods and (ii) defect healing by the polymer within the rod microporosity, which fills pre-existing defects in the β-TCP rods, bonding the defect walls together, and thus increasing the stress needed for a crack to propagate from them. Obviously, the stress shielding component is suppressed in the coated, TCP/PCL^C, structures since the macroporosity remains virtually intact. Therefore, the strengthening factor of 2.2 ± 0.4 estimated for TCP/PCL^C structures (Fig. 7) is associated solely to the defect healing mechanism. Assuming that the effectiveness of the healing is similar in TCP/PCL structures, the strengthening associated to stress shielding, indicated as a patterned band in the corresponding column (TCP/PCL) of Figure 7, is estimated as 1.2 ± 0.4. This agrees completely with the results of FEM simulations performed for bare and fully impregnated structures (Fig. 8). Indeed, the FEM-based calculation of the strengthening factor associated to stress shielding by PCL full infiltration is of 1.2 ± 0.2, in perfect agreement with the estimation from the experimental results in Figure 7. This confirms the hypothesis that the defect-healing effect is similar in TCP/PCL^C and TCP/PCL scaffolds. Further evidence of this can be found in the fact that the Weibull modulus evaluated in both type of hybrid structures is virtually the same (m = 5.2 ± 0.2 vs. 5.0 ± 0.3, respectively), which indicates that a similar starting flaw population exists in TCP/PCL^C and TCP/PCL systems. The good agreement between the FEM predictions and experimental data confirms once more[31,36] the reliability of this technique as a tool for predicting the stress fields in these complex structures.

The strength increase after coating with PCL evidenced in Figure 7 (120%) is much larger than previously reported results for conventional scaffolds with similar total porosities coated by immersion in PCL solution (∼15–30%[16]). And the level of strengthening could even be increased further if higher polymerization temperatures and times were used.[20] Nonetheless, since the scaffold geometries and

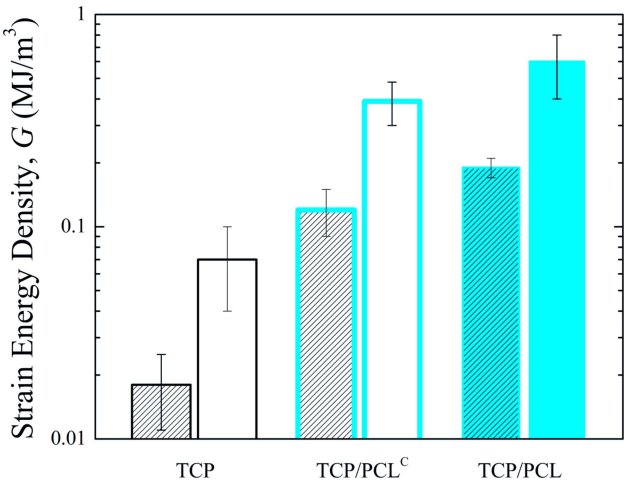

FIGURE 9. Strain energy density, G, data from compression tests in PCL-coated structures (TCP/PCL^C). Data for bare (TCP) and PCL fully impregnated (TCP/PCL) structures from previous work[19] are included for comparison. For each type of structure, left (patterned) bars represent G_{max} values, whereas right bars correspond to $G_{0.1}$. Error bars represent standard deviations. [Color figure can be viewed in the online issue, which is available at wileyonlinelibrary.com.]

materials are not the same in all these studies, all these data comparisons should be treated with care.

On the other hand, the mechanical performance enhancement provided by polymer infiltration is not limited to strength and reliability but extends also to toughness. As shown in Figure 9, TCP/PCL^C and TCP/PCL scaffolds exhibit, independently of the strain considered, a strain energy density in compression at least five times (400%) higher than the bare TCP structures, with the TCP/PCL^C structures exhibiting slightly lower values. This enhancement is, again, far superior to that reported in solution-impregnated conventional scaffolds by other authors (<70%).[16] The toughening can be attributed on the one hand to the strengthening provided by the polymer infiltration, and on the other to polymeric fibrils that bridge the crack walls and hold the structure together after the ceramic skeleton fails.[16] The reduced toughness of TCP/PCL^C compared to TCP/PCL structures is clearly due to the lack of polymer within the macropores, which negatively affect both contributions. Indeed, the polymer in the macropores is able to hold the structure together even after large deformations, with fully impregnated samples preserving mechanical integrity after 30% strains, while simply coated structures break into pieces before that. In spite of that, Figures 3(c) and 4(b) show that polymer fibrils on scaffold fracture surfaces are short, indicating that crack bridging mechanism is not very effective with the current processing conditions, thus, most of the observed toughening is in fact a product of the strengthening achieved. The bridging mechanism could be enhanced, nonetheless, by increasing the molecular weight, and thus the ductility, of the infiltrating PCL polymer.[16]

To sum up, deposition of a polymer coating has been demonstrated to be an excellent means to improve the mechanical performance of bioceramic robocast scaffolds while preserving the predesigned macroporosity architecture, with its high degree of interconnectivity. Both strength and toughness were increased substantially over the values of bare scaffolds, and in the case of the strength, up to values that clearly surpass those corresponding to cancellous bone (<5 MPa), although still fall short of those corresponding to cortical bone (30–250 MPa).[37] Obviously, the improvement on the mechanical performance achieved will depend on the intrinsic properties of the coating material: elastic modulus, strength, toughness and adhesion strength to the scaffold material.

Nonetheless, it is worth mentioning that deposition of a fully homogeneous coating over the bioceramic scaffold surface could reduce its bioactivity and affect cell adhesion since the calcium and phosphate ions would not be exposed to the biological environment until the polymer was resorbed. A possible solution to this drawback would be to adjust the coating process to produce infiltration of in-rod microporosity but without fully covering the external surface of the rods to preserve some of the superficial calcium phosphate material. Nevertheless, while achieving this is deemed feasible, it would be technically difficult and, most probably, reducing the polymer surface coverage would result in a reduced healing of rods' defects, which will translate into a reduced mechanical performance. A balance between both key aspects, mechanical and biological performances, would have to be achieved. An alternative solution to improve the biological performance without jeopardizing the mechanical properties would be to incorporate growth factors into the polymer formulation or bioceramics as reinforcing nanoparticles within the polymer (thus using a nanobiocomposite as infiltrating material). The use of a nanobiocomposite as the infiltrating material would also be appealing for the improvement of the mechanical performance of the coating, and this possibility would be analyzed in future works.

Finally, it is worth mentioning, that the fabrication process proposed here has been tuned to optimize exclusively the mechanical performance of the resulting coated scaffold, to show the potential benefits of this strategy. Modifications of the process would probably be required in order to warrant a suitable biological response. For example, additional washing and scouring steps would be required to eliminate potentially harmful remnants of the toluene solvent. Alternatively, an additional heat treatment could be used to simultaneously eliminate such remnants and to sterilize the scaffold, although obviously this additional treatment might modify the mechanical response and complicate the addition of biomolecules to the coating. Additional care might be taken also in avoiding excessive residual unreacted monomers to prevent possible toxicological effects, although ε-CL exhibits low acute toxicity.[38]

CONCLUSIONS AND IMPLICATIONS

Infiltrating bioceramic scaffolds with a biodegradable polymer (PCL) to produce a homogeneous coating has been demonstrated to be an excellent means to improve the scaffold's mechanical performance, both in terms of strength and toughness, while preserving the predesigned pore architecture produced by robocasting. In this sense, the method utilized here, ISP, has demonstrated to be an excellent choice to develop highly homogeneous PCL films and to completely seal the scaffold microdefects. The selection of the appropriate coating material might allow one to improve the mechanical performance even further.

Nonetheless, if mechanical properties were the only concern, fully impregnating the structures would be a more efficient reinforcement strategy. In that case, the necessary porosity to allow cell ingrowth would have to be created *in situ* during the scaffold biodegradation, which remains a scientific challenge. However, preserving the predesigned macroporosity by applying just a coating will facilitate bone ingrowth into the hybrid scaffold from the beginning, and enable seeding of the scaffold with appropriate cell lines prior to implantation. This possibility may be important when repairing large defects in order to avoid, or at least to hamper, the colonization of the scaffold by undesired cell types, typically fibroblastic, with higher migration or proliferation rates than the target cells.

At any rate, the results of this work provide valuable insight into the mechanical behavior of hybrid ceramic/

polymer scaffolds for bone tissue engineering applications, and pave the way to achieving more appropriate implants for bone regeneration.

REFERENCES

1. Langer R, Vacanti JP. Tissue Engineering. Science 1993;260: 920–926.
2. Hollister SJ. Porous scaffold design for tissue engineering. Nat Mater 2005;4:518–524.
3. Williams JM, Adewunmi A, Schek RM, Flanagan CL, Krebsbach PH, Feinberg SE, Hollister SJ, Das S. Bone tissue engineering using polycaprolactone scaffolds fabricated via selective laser sintering. Biomaterials 2005;26:4817–4827.
4. Chen QZZ, Thompson ID, Boccaccini AR. 45S5 Bioglass (R)-derived glass–ceramic scaffolds for bone tissue engineering. Biomaterials 2006;27:2414–2425.
5. Chevalier J, Gremillard L. Ceramics For medical applications: A picture for the next 20 years. J Eur Ceram Soc 2009;29:1245–1255.
6. Tamai N, Myoui A, Tomita T, Nakase T, Tanaka J, Ochi T, Yoshikawa H. Novel hydroxyapatite ceramics with an interconnective porous structure exhibit superior osteoconduction in vivo. J Biomed Mater Res 2002;59:110–117.
7. Freyman TM, Yannas IV, Gibson LJ. Cellular materials as porous scaffolds for tissue engineering. Prog Mater Sci 2001;46:273–282.
8. Fu Q, Saiz E, Rahaman MN, Tomsia AP. Bioactive glass scaffolds for bone tissue engineering: State of the art and future perspectives. Mater Sci Eng C 2011;31:1245–1256.
9. Boccaccini AR, Blaker JJ. Bioactive composite materials for tissue engineering scaffolds. Expert Rev Med Device 2005;2:303–317.
10. Hon KKB, Li L, Hutchings IM. Direct writing technology: Advances and developments. CIRP Ann: Manuf Technol 2008;57:601–620.
11. Cesarano J III, Segalman JR, Calvert P. Robocasting provides moldless fabrication from slurry deposition. Ceram Ind 1998;148: 94–102.
12. Miranda P, Saiz E, Gryn K, Tomsia AP. Sintering and robocasting of beta-tricalcium phosphate scaffolds for orthopaedic applications. Acta Biomater 2006;2:457–466.
13. Smay JE, Cesarano J, Lewis JA. Colloidal inks for directed assembly of 3-D periodic structures. Langmuir 2002;18:5429–5437.
14. Miranda P, Pajares A, Saiz E, Tomsia AP, Guiberteau F. Mechanical properties of calcium phosphate scaffolds fabricated by robocasting. J Biomed Mater Res Part A 2008;85A:218–227.
15. Peroglio M, Gremillard L, Chevalier J, Chazeau L, Gauthier C, Hamaide T. Toughening of bio-ceramics scaffolds by polymer coating. J Eur Ceram Soc 2007;27:2679–2685.
16. Peroglio M, Gremillard L, Gauthier C, Chazeau L, Verrier S, Alini M, Chevalier J. Mechanical properties and cytocompatibility of poly(epsilon-caprolactone)-infiltrated biphasic calcium phosphate scaffolds with bimodal pore distribution. Acta Biomater 2010;6: 4369–4379.
17. Komlev VS, Barinov SM, Rustichelli F. Strength enhancement of porous hydroxyapatite ceramics by polymer impregnation. J Mater Sci Lett 2003;22:1215–1217.
18. Martinez-Vazquez FJ, Perera FH, Miranda P, Pajares A, Guiberteau F. Improving the compressive strength of bioceramic robocast scaffolds by polymer infiltration. Acta Biomater 2010;6:4361–4368.
19. Martinez-Vazquez FJ, Perera FH, Van Der Meulen I, Heise A, Pajares A, Miranda P. Impregnation of β-tricalcium phosphate robocast scaffolds by in-situ polymerization. J Biomed Mater Res Part A. DOI: 10.1002/jbm.a.34609.
20. Walsh D, Furuzono T, Tanaka J. Preparation of porous composite implant materials by in situ polymerization of porous apatite containing E-caprolactone or methyl methacrylate. Biomaterials 2001; 22:1205–1212.
21. Asmus SMF, Nakahira A, Pezzotti G. Manufacture and bioactivity of tough hydroxyapatite/nylon hybrid composites. Adv Compos Mater 2003;11:255–264.
22. Nakahira A, Tamai M, Miki S, Pezzotti G. Fracture behavior and biocompatibility evaluation of nylon-infiltrated porous hydroxyapatite. J Mater Sci 2002;37:4425–4430.
23. Pezzotti G, Asmus SMF. Fracture behavior of hydroxyapatite/polymer interpenetrating network composites prepared by in situ polymerization process. Mater Sci Eng A 2001;316:231–237.
24. Pezzotti G, Asmus SMF, Ferroni LP, Miki S. In situ polymerization into porous ceramics: A novel route to tough biomimetic materials. J Mater Sci: Mater Med 2002;13:783–787.
25. Kobayashi S, Takeya K, Suda S, Uyama H. Lipase-catalyzed ring-opening polymerization of medium-size lactones to polyesters. Macromol Chem Phys 1998;199:1729–1736.
26. Kobayashi S, Uyama H. Precision enzymatic polymerization to polyesters with lipase catalysts. Macromol Symp 1999;144: 237–246.
27. Perera FH, Martinez-Vazquez FJ, Miranda P, Ortiz AL, Pajares A. Clarifying the effect of sintering conditions on the microstructure and mechanical properties of beta-tricalcium phosphate. Ceram Int 2010;36:1929–1935.
28. Albertsson AC, Varma IK. Recent developments in ring opening polymerization of lactones for biomedical applications. Biomacromolecules 2003;4:1466–1486.
29. De Geus M, Peeters J, Wolffs M, Hermans T, Palmans ARA, Koning CE, Heise A. investigation of factors influencing the chemoenzymatic synthesis of block copolymers. Macromolecules 2005;38: 4220–4225.
30. Kumar A, Gross RA. *Candida antartica* lipase B catalyzed polycaprolactone synthesis: Effects of organic media and temperature. Biomacromolecules 2000;1:133–138.
31. Miranda P, Pajares A, Guiberteau F. Finite element modeling as a tool for predicting the fracture behavior of robocast scaffolds. Acta Biomater 2008;4:1715–1724.
32. Weibull W. A statistical distribution function of wide applicability. J Appl Mech: Trans ASME 1951;18:293–297.
33. Grenoble DE, Dunn KL, Katz JL, Gilmore RS, Murty KL. Elastic properties of hard tissues and apatites. J Biomed Mater Res 1972; 6:221–233.
34. Chen BQ, Evans JRG. Poly(epsilon-caprolactone)–clay nanocomposites: Structure and mechanical properties. Macromolecules 2006;39:747–754.
35. Miranda P, Pajares A, Saiz E, Tomsia AP, Guiberteau F. Fracture modes under uniaxial compression in hydroxyapatite scaffolds fabricated by robocasting. J Biomed Mater Res Part A 2007;83A: 646–655.
36. Norato J, Johnson A. A computational and cellular solids approach to the stiffness-based design of bone scaffolds. J Biomech Eng: Trans ASME 2011;133.
37. Keller TS. Predicting the compressive mechanical-behavior of bone. J Biomech 1994;27:1159–1168.
38. ε-Caprolactone. Report From "Screening Information Data Set" (SIDS) Program. Organization for Economic Cooperation and Development (OECD); 2004. http://www.Chem.Unep.Ch/Irptc/Sids/Oecdsids/502443.Pdf